OMAE2021-62542

SYSTEM UNCERTAINTY EFFECTS ON THE WAVE FREQUENCY RESPONSE OF FLOATING VESSELS BASED ON POLYNOMIAL CHAOS EXPANSION

Gowtham Radhakrishnan, Xu Han, Svein Sævik, Zhen Gao, Bernt Johan Leira
Department of Marine Technology, Centre for Marine Operations in Virtual Environments (SFI MOVE)
Norwegian University of Science and Technology
Trondheim, Norway

ABSTRACT

From a mathematical viewpoint, the frequency domain analysis of vessel motion responses due to wave actions incorporates the integration of system dynamics idealized in terms of response amplitude operators (RAOs) for 6 DOF rigid body motions and an input wave spectrum to yield the response spectrum. Various quantities of interest can be deduced from the response spectrum and further used for decision support in marine operations, extreme value and fatigue analysis. The variation of such quantities, owing to the uncertainties associated with the vessel system parameters, can be quantified by performing uncertainty propagation (UP) and consequent sensitivity analysis (SA). This study, emphasizes and proposes a computational-efficient way of assessing the sensitivity of the system model output with respect to the uncertainties residing in the input parameters by operating on a surrogate model representation. In this respect, the global sensitivity analysis is effectively carried out by deploying an efficient non-intrusive polynomial chaos expansion (PCE) surrogate model built using a point collocation strategy. Successively, the coherent and effective Sobol' indices are obtained from the analytical decomposition of the polynomial coefficients. The indices, eventually, are employed to quantitatively gauge the effects of input uncertainties on the output 6 DOF vessel responses.

Keywords: frequency domain analysis, polynomial chaos expansion, uncertainty propagation, sensitivity analysis, Sobol' indices

NOMENCLATURE

FD	Frequency Domain
C3S	Copernicus climate change service
CDS	Climate Data Store
QoI	Quantities of Interest
UP	Uncertainty Propagation
SA	Sensitivity Analysis
PCE	Polynomial Chaos Expansion
RMS	Root mean square
CoG	Center of Gravity
XCG	Longitudinal coordinate of CoG
YCG	Transverse coordinate of CoG
ZCG	Vertical coordinate of ZCG
M	Vessel mass
I_{44}	Roll moment of inertia
I_{55}	Pitch moment of inertia
I_{66}	Yaw moment of inertia
β_{33}	Additional linearized heave damping coefficient
β_{44}	Additional linearized roll damping coefficient
β_{55}	Additional linearized pitch damping coefficient
$\beta_{33,cr}$	Critical heave damping coefficient
$\beta_{44,cr}$	Critical roll damping coefficient
$\beta_{55,cr}$	Critical pitch damping coefficient
Q	Independent physical space inputs
X	Independent/Correlated physical space inputs
U	Independent inputs in standard normal space
OLS	Ordinary Least Squares

1. INTRODUCTION

The usual practice to predict the behavior of a physical asset (ship/offshore structures) in the open ocean is to establish a representative computational model and perform numerical evaluations. The computational model is solely based on solving

the differential equations that satisfy the governing physics. To this end, in the present paper, the main focus is dedicated towards the employment of the frequency domain approach for the vessel response evaluation. On the negative side, this model is based on numerous assumptions on initial and boundary conditions, together with the consideration of linearity properties, and thereby the resulting predictions may deviate considerably from the real physical behavior. Equally important are the uncertainties associated with the metocean characteristics that impart appreciable randomness to the vessel behavior. Thus, from an operational viewpoint, it is regarded vital to account for the uncertainties arising from all sources to quantitatively assess their relative effects on the response quantities of interest and make crucial operational decisions. In the current paper, the primary response quantities of interest (QoI) are the response RMS of 6 DOF rigid body motions. With that being said, the central focus is dedicated towards the evaluation of sensitivities of vessel QoIs with respect to each input uncertainty and the underlying interactions between them. The input uncertainty, here, particularly refers to the system uncertainty, (i.e) system parameters will be modelled as random variables and consequent effects on the response will be studied.

In view of assessing the effects of input uncertainty on the model response, two different classes of methods can be adopted. *Regression-based methods* use regression coefficients to assess the input uncertainty effect on the output. In other words, the relationships and correlation between the input and the output quantities are estimated, which, in turn are utilized to measure the uncertainty. These methods have some serious drawbacks in that they are effective only when there exists a linear relationship between the input and output. In presence of a strong non-linear connection, their predictions in relation to response sensitivity deteriorate and become rather questionable. The other class of methods, known as *Variance based methods,* or widely called as *Analysis of Variance,* make use of indices that measure the resulting model sensitivity by representing the conditional variance of the output with respect to each uncertain input parameter and various combinations of them. Unlike the regression methods, the variance-based indices are known to be effective for non-linear problems as well. Fourier amplitude sensitivity test (FAST) indices and Sobol' indices fall into this family. In the present study, prominent attention is given to the usage of Sobol' indices. The conventional way of estimating Sobol' indices is to perform a full Monte Carlo analysis involving few thousand high-fidelity runs. In this respect, the indices' calculation aggravates the problem of computational complexity, if the primary physical model is computationally expensive to evaluate [1].

Sudret (2007) developed a theoretical framework through which the Sobol' indices can be estimated from the polynomial coefficients in a cost-efficient way and employed the same for assessing the sensitivity of a foundation model [1]. Soon after its development, successful applications of polynomial based global sensitivity analysis have been achieved in different disciplines.

To quote a few, Blatman (2007) applied this on truss & frame structural models, Deman et al. (2016) performed sensitivity analysis with 78 input variables in the field of hydrogeology, Mai(2016) applied this concept for uncertainty analyses in the field of earthquake engineering [2] [3] [4]. Nonetheless, in Marine Technology, so far, very few uncertainty studies involving PCE have been carried out. Even those studies, are mostly restricted to applications within slender marine structures, refer Sauder (2018), Pinghe Ni et al. (2017) & Paredes et al. (2020) [5] [6] [7]. Wei et al. (2019) conducted a sensitivity study using PCE and performed subsequent uncertainty optimization on a bulk carrier model [8].

Having stated the previous works in Marine engineering using PCE, a novel attempt is initiated, as part of this study, to utilize the potential capabilities of PCE surrogates as part of onboard decision support systems for offshore supply vessels. The results will be utilized as a basis for conducting surrogate-assisted model calibration using actual vessel measurements. In other words, highly sensitive parameters relative to each response mode are properly identified and subjected to calibration while disregarding the parameters that are of little significance.

Section 2 discusses the theoretical framework related to the frequency domain analysis, background on global sensitivity analysis, polynomial chaos expansions and obtaining Sobol' indices from PCE. Section 3 describes the practical steps involved in performing the uncertainty study. Section 4 starts with the selection of the optimal surrogate through proper convergence study, followed by the elaborate discussions on the influence of system uncertainties on the model response. Decisive inferences on utilization of the obtained results for model calibration are given in the conclusion section.

2. THEORY

2.1 Frequency domain analysis

DNV-GL (2010) presents the semi-empirical structure of Jonswap spectrum as a peak enhanced Pierson-Moskowitz spectra given as [9]:

$$S_\zeta(\omega) = A_\gamma \frac{5}{16} Hs^2 \omega_p^4 \omega^{-5} e^{\left(-\frac{5}{4}\left(\frac{\omega}{\omega_p}\right)^{-4}\right)} \gamma^{\left(-0.5\left(\frac{\omega-\omega_P}{\sigma\omega_P}\right)^2\right)} \quad (1)$$

where Hs represents the significant wave height, $\omega_p = \frac{2\pi}{Tp}$ denotes the angular spectral peak frequency, with Tp being the wave peak period. γ is the non-dimensional peak shape parameter with an average value of 3.3. σ denotes the spectral width parameters with $\sigma = \sigma_a$ for $\omega \leq \omega_P$ and $\sigma = \sigma_b$ for $\omega > \omega_P$. A_γ is a normalizing factor with a value equal to $1 - 0.287ln(\gamma)$. Also, if the $\frac{TP}{\sqrt{H_S}}$ value is greater than 5, it has been suggested to use $\gamma = 1$.

In open ocean, the wave energy is spread around the main wave propagation direction, i.e resulting in short-crested seas. Accordingly, the effect due to the directional nature of energy spread, can properly be represented in the calculations only through translation of the 1 D spectrum into a directional spectrum based on the expression contained in Eq.2 [10].

$$D(\theta) = \frac{2}{\pi}cos^2(\theta - \theta_R) \text{ for } -\frac{\pi}{2} + \theta_R \text{ to } \frac{\pi}{2} + \theta_R \rbrace$$
$$And \ 0 \ otherwise \qquad (2)$$

The relative wave heading/direction, θ_R, defined with respect to mathematical vessel axis is given as [11]

$$\theta_R = 180 + V_\theta - \theta_M \qquad (3)$$

θ_M is the mean wave direction defined according to oceanographic-axis conventions, 0° as waves coming from the North and 180° as waves coming from the South [12]. V_θ is the vessel heading, which is also defined clockwise from the reference North. The addition of 180 is to convert the oceanographic based axis to the mathematical vessel coordinate system followed in transfer function computations, since the latter considers 180° as head waves and 0° as following waves. This concept is illustrated in Figure 1.
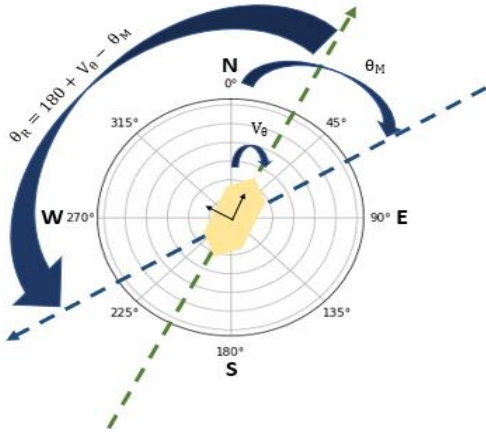
Figure 1 Representation of relative wave direction, θ_R, calculated with respect to vessel's mathematical coordinate system, is shown graphically for a V_θ close to 30° and θ_M close to 60°.

Successively, $S_\zeta(\omega,\theta) = S_\zeta(\omega)D(\theta) \qquad (4)$

The setup in Eq.4 presents the 2D wave spectral formulation. The motion transfer function from the wave elevation ζ at a reference point to the motion response Z can be written as follows:

$$H_{\zeta Z}(\omega,\theta) = H_{FZ}(\omega).H_{\zeta F}(\omega,\theta) \qquad (5)$$

$H_{FZ}(\omega) = \left(\left(-\omega^2\left(\bar{\bar{M}} + \bar{\bar{A}}(\omega)\right) + i\omega\bar{\bar{B}}(\omega) + \bar{\bar{C}}\right)\ \right)^{-1}$ represents the transfer function from the first order wave load F to the motion response Z and $H_{\zeta F}(\omega,\theta)$ is the transfer function from the wave elevation ζ at a reference point to the first order wave load F. $\bar{\bar{M}}$ is the mass matrix, $\bar{\bar{A}}$ refers to the added mass matrix, $\bar{\bar{B}}$ represents the damping matrix, $\bar{\bar{C}}$ denotes the stiffness matrix [13]. The absolute value $\left|H_{\zeta Z}(\omega,\theta)\right|$ is employed in Eq.6. Usage of 3D panel method, a technique belonging to the family of potential flow based approaches, has been considered for deriving solutions to the above mentioned equations, for vessels with zero mean forward speed. It uses the Green's theorem to reduce the three-dimensional potential equation to a two-dimensional surface integral equation. Then, the corresponding solution to integrals can be obtained by distribution of sources on the surface [14]. Wamit 7, a hydrodynamic code, based on boundary element method has been employed for the computations [15].

The 2D response spectrum $S_y(\omega,\theta)$ can, then, be formulated as in Eq.6. Performing integration along the directional axis results in the 1D response spectrum $S_y(\omega)$. A successive integration along the frequency axis produces the zero-order spectral moment m_0. Finally, the root mean square (RMS) value, the primary quantity of interest in this study, can be evaluated by taking the square root of m_0. Relevant equations are as follows:

$$S_y(\omega,\theta) = S_\zeta(\omega,\theta)\left|H_{\zeta Z}(\omega,\theta)\right|^2 \qquad (6)$$

$$S_y(\omega) = \int_0^{2\pi} S_y(\omega,\theta)\,d\theta \qquad (7)$$

$$RMS = \sqrt{m_0} = \sqrt{\int_0^\infty S_y(\omega)d\omega} \qquad (8)$$

2.2 Global sensitivity analysis using Sobol' indices

Sobol' indices are variance-based measures that can quantify the model response variation with respect to the influence of each uncertain input parameter along with the effects arising from the occurrence of underlying interactions among the random parameters.

Let us consider that the output response of a model subjected to probabilistic inputs can be represented in the form [3]:

$$Y = \mathcal{M}(Q) = \mathcal{M}_0 + \sum_{i=1}^D \mathcal{M}_i(Q_i) + \sum_{1 \leq i < j \leq D} \mathcal{M}_{ij}(Q_i, Q_j) +$$
$$\ldots + \mathcal{M}_{1,\ldots,D}(Q) = \mathcal{M}_0 + \sum_{l \neq \emptyset} \mathcal{M}_l(Q_l) \qquad (9)$$

Where Q represents the vector of different independent random inputs. It signifies the physical space inputs and should necessarily be independent and D is the number of input variables. $\mathcal{M}_0$ denotes the mean value of response. $l = \{i_1, \ldots, i_s\} \subset \{1, \ldots, D\}$ represents the index sets. Q_l is a subvector of Q, which consists only of elements with indices corresponding with the index set l [3]. The decomposition of the variance of the output $\mathcal{M}(Q)$, on the condition that $\mathcal{M}(Q)$ satisfies the orthogonality property, can be written as [16, 17]:

$$V = Var[\mathcal{M}(Q)] = \sum_{i=1}^D V_i + \sum_{1 \leq i < j \leq D} V_{ij} + \cdots +$$
$$V_{1,\ldots,D} = \sum_{l \neq \emptyset} V_l \qquad (10)$$

On dividing the individual terms in Eq.10 by the total variance V,

$$\sum_{i=1}^{D} S_i + \sum_{1 \le i < j \le D} S_{ij} + \cdots + S_{12\ldots D} = \sum_{l \ne \emptyset} S_l = 1 \qquad (11)$$

The items S give the sensitivity of the output response in relation to the uncertain input parameters. The total sensitivity should be equal to 1, which is composed of the main effects and interactions. From Eq.11, the first order sensitivity indices or the main effects are given as *[16]*:

$$S_i = \frac{V[E[Y|Q_i]]}{V[Y]} \qquad (12)$$

These indices identify the individual effects of each uncertain parameters on the model response without considering the interactions. The second order indices, S_{ij}, measure the interactions between the random inputs (Q_i, Q_j) and report their ensuing effects on the output. Mathematically, they can be framed as [16]:

$$S_{i,j} = \frac{V[E[Y|Q_i,Q_j]]}{V[Y]} - S_i - S_j \qquad (13)$$

The remaining extensions in Eq.11 correspond to the higher order indices, which gauge the effects on the model response due to interactions among larger combination of input random variables [3]. Calculation of higher-order indices demands extreme computational work and nearly impossible for higher-dimensional problems [5].

The total sensitivity indices quantify the complete effect of the parametric uncertainty on the model response, i.e. including first order effects and all interactions. Owing to the complex computations associated with the estimation of higher order sensitivity indices in Eq.11, most often, the total sensitivity index of a variable i is computed using the simple expression contained in Eq.14. [17] [16]

$$S_{T,i} = 1 - \frac{V[E[Y|Q_{\sim i}]]}{V[Y]} \qquad (14)$$

$Q_{\sim i}$, denotes all other input parameters other than Q_i. The normal practice, in most sensitivity studies, is to evaluate the first order and total order indices [16]. Traditionally, the Monte Carlo approach is used to estimate the Sobol' indices [1] [16] [17]. The Monte Carlo approach demands a larger number of simulation runs to obtain a reasonable value for these indices. In order to circumvent this problem, Sudret (2007), proposed a computational efficient procedure by obtaining the Sobol' indices directly from the polynomial coefficients by means of Polynomial Chaos Expansion (PCE). This is based on the fact that PCE possess orthogonal properties which is an important requirement for carrying out Sobol' decomposition. [1] [2] [5].

2.3 Polynomial Chaos Expansion

According to polynomial chaos expansion (PCE), the probabilistic response behavior of a physics-based model can be represented as an expansion series consisting of orthogonal polynomials as follows [1]:

$$Y = \mathcal{M}(X) \approx \mathcal{M}_{PC}(U) = \sum_{\alpha=0}^{\infty} c_\alpha \Psi_\alpha(U) \qquad (15)$$

Where $Y = \{y_1, \ldots, y_T\} \in R^T$, contains the output quantities of interest (here $T \ge 1$), which in this paper imply RMS value of each output response component. X represents the physical input space which can either be independent or correlated. The PC surrogate ($\mathcal{M}_{PC}$) functions on the independent standard space variables, therefore, standard probabilistic transformation techniques can be pursued for variable mapping from one space to another. $\Psi_\alpha(U)$ indicates multivariate polynomials, that are orthonormal with respect to the standard probability space of independent input variables ($f_U(u)$). So $E[\psi_a \psi_\beta] = \delta_{\alpha\beta}, \delta_{\alpha\beta} = 1 \; if \; \alpha = \beta, 0 \; if \alpha \ne \beta$. c_α signifies the polynomial coefficients. In the current work, it is of especial interest to employ orthonormal Hermite polynomials defined on the standard normal space(U) with zero mean and unit variance. From the computational point of view, it is considered practical to reduce the infinite expansion series in Eq. 15 to a finite number of terms. Following this fact, the series is truncated to P terms where P denote $\frac{(D+p)!}{D!p!}$. D refers the number of input variables/input dimensions and p is the highest p-th order term of the Hermite polynomials [1] [2] [3] [18]

$$Y \approx \sum_{\alpha=0}^{P-1} c_\alpha \Psi_\alpha(U) = \mathcal{M}_{PC}(U), \alpha \in A \qquad (16)$$

Here, A denotes a multi-indices set $\alpha = (\alpha_1, \ldots, \alpha_D)$. Successively, the orthogonality property of the polynomial bases facilitates the computation of statistical moments from the polynomial coefficients. Theoretical representations for deducing the mean from polynomial coefficients is presented in Eq.17 [2] [3].

$$\mu_{PC} = E[\mathcal{M}_{PC}(U)] = c_0 \qquad (17)$$

The variance is computed by [5]

$$\mathcal{M}_{PC}(U) - E[\mathcal{M}_{PC}(U)] = \sum_{\alpha=1}^{P-1} c_\alpha \Psi_\alpha(U) \qquad (18)$$

$$V_{PC} = Var[\mathcal{M}_{PC}(U)] = E[(\mathcal{M}_{PC}(U) - E[\mathcal{M}_{PC}(U)])^2] \qquad (19)$$

$$V_{PC} = \sum_{\alpha=1}^{P-1} c_\alpha^2 E[\psi_\alpha^2(U)] = \sum_{\alpha=1}^{P-1} c_\alpha^2 \qquad (20)$$

The skewness and kurtosis coefficients can be effectively computed using the formulations in Eq.21 & Eq.22

$$\delta_{PC} = \frac{1}{\sigma_{PC}^3} E[(\mathcal{M}_{PC}(U) - \mu_{PC})^3] \qquad (21)$$

$$\kappa_{PC} = \frac{1}{\sigma_{PC}^4} E[(\mathcal{M}_{PC}(U) - \mu_{PC})^4] \qquad (22)$$

Here, the standard deviation, $\sigma_{PC} = \sqrt{V_{PC}}$. Eq.21 & Eq.22 are cost effective alternatives to the conventional way of evaluating skewness and kurtosis from Hermite polynomials [2]. From the surrogate representations, the response PDF can also be obtained in addition to the statistical moments. This is achieved by conducting 'N_u' Monte Carlo runs on the polynomial model, followed by constructing a kernel formulation based on the resulting response values [2] [18].

$$\hat{f}_Y(\hat{y}) = \frac{1}{N_u h} \sum_{j=1}^{N_u} K\left(\frac{\hat{y} - \hat{y}^{(j)}}{h}\right) \qquad (23)$$

Where K is a positive kernel function and h represents the bandwidth parameter. N_u represents the large sample size extracted from the standard probability space. $\hat{y}^{(j)} = \mathcal{M}_{PC}(u^{(j)}), j = 1,2, \dots, N_u$.

Quasi-Random sequences:
Evaluation of polynomial coefficients mandates stochastic response output from the actual frequency domain model for different combinations of uncertain inputs. For this purpose, the experimental design samples from the input probability space are obtained using Quasi-random/low-discrepancy sequences. These sequences are pursued to achieve a fast convergence rate. Strong attention is devoted towards the usage of Sobol' sequences owing to its efficiency in handling higher-dimensional problems($D \geq 10$). An one-dimensional Sobol' sequence is represented using the following expression [2]

$$v^{(i)} = \frac{b_0}{2} + \frac{b_1}{2^2} + \dots + \frac{b_m}{2^{m+1}}, \ b_n \in \{0,1\} \qquad (24)$$

The Sobol' sequence can be extended to 'D' dimensions by carrying out D permutations of the one-dimensional sequence. Usually, the collocation points are generated from the standard normal space and transformed to points in physical space, which, in turn are used to perform simulations on the high-fidelity model [1].

Computing the coefficients:
Constructing a PCE model by making use of the point collocation approach is of main interest. With regards to this, the coefficients are estimated based on the principle of least squares minimization, which is a regression-oriented approach.

$$Y = \mathcal{M}(X) = \sum_{\alpha=0}^{P-1} c_\alpha \Psi_\alpha(U) + \varepsilon \qquad (25)$$

Here, the term ε represent the residual error with zero mean. Consequently, the coefficients c_α, are computed so that they minimize the difference between the approximation and the actual response, which can be obtained by [1]:

$$argminE\left[\left(\mathcal{M}(X) - c^T \Psi(U)\right)^2\right] \qquad (26)$$

2.4 Sobol' decomposition of Polynomial Chaos Expansion

Having reformulated the actual model output in the form of polynomial basis functions as in Eq.16, the multivariate polynomials, $\Psi_\alpha(U)$, can be presented as a tensor product of the univariate polynomials associated with each input variable.

$$\Psi_\alpha(U) = \prod_{i=1}^{D} \psi_{\alpha_i}{}^{(i)}(U_i) \qquad (27)$$

Where $\psi_{\alpha_i}{}^{(i)}$ is the polynomial in the i-th input variable that are orthonormal with respect to $f_{U_i}(u_i)$. Where $f_{U_i}(u_i)$, $i=1,2,\dots D$, represent the marginal PDFs. Let us define the set of multi-indices A_l which corresponds to the index set l, $A_l = \{\alpha \in A: \alpha_k \neq 0, k \in l, l = \{i_1, \dots, i_s\} \subset \{1, \dots, D\}\}$. It follows that $\cup A_l = A$(in Eq. 16). The derivation of the Sobol' indices – the first, second and total order indices, can effortlessly be achieved by performing basic operations on the polynomial coefficients as follows [3].

$$\text{1st order-} \ \widehat{S}_i = \sum_{\alpha \in A_i} \frac{c_\alpha^2}{V_{PC}}, \ A_i = \{\alpha \in A: \alpha_i > 0, \alpha_{j \neq i} = 0\} \qquad (28)$$

$$\text{2nd order-} \ \widehat{S}_{ij} = \sum_{\alpha \in A_{ij}} \frac{c_\alpha^2}{V_{PC}}, \ A_{ij} = \begin{cases} \alpha \in A: \alpha_i, \alpha_j > 0 \\ , \alpha_{k \neq i,j} = 0 \end{cases} \qquad (29)$$

$$\text{Total Order -} \ \widehat{S}_i^T = \sum_{\alpha \in A_i^T} \frac{c_\alpha^2}{V_{PC}}, A_i^T = \{\alpha \in A: \alpha_i > 0\} \qquad (30)$$

2.5 Sparse polynomial chaos expansions

The PC expansion scheme presented in Eq.16, which itself has only finite number of terms, becomes cumbersome to deal with for higher dimensional problems owing to the huge number of generated expansion terms in compliance with the increasing polynomial order and random variables. The amount of high-fidelity simulation runs for a reliable sensitivity study must concur with the following qualitative thumb rule [18]:

$$N \geq 2 * ExpansionTerms \ (P) \qquad (31)$$

Simulation numbers smaller than this limit will probably result in an under determined system. Extensive PC expansions, therefore, demand massive computational runs. As a means to deal with this problem, the following approach is also pursued in this paper.

Hyperbolic Truncation : As per this truncation strategy, the PC expansion terms in Eq 16. can be reduced by setting proper q-norms according to Eq.32: [2] [3]

$$\|\alpha\|_q = \left(\sum_{i=1}^{D} \alpha_i^q\right)^{1/q} \leq P \qquad (32)$$

Specification of q-norm dictates the quantity of truncation. When $q = 1$, the number of terms will be identical to that of Eq.16. By having reduced norm values between $0 < q < 1$, the number of terms will be minimized accordingly. q value lesser than 1 reduces the quantity of basis terms representing the interaction between the variables [3]. The preserved terms, after truncation, happen to fall under a hyperbola, hence, the term *hyperbolic truncation* is applied. *An illustration of the concept* is given in Figure 2.
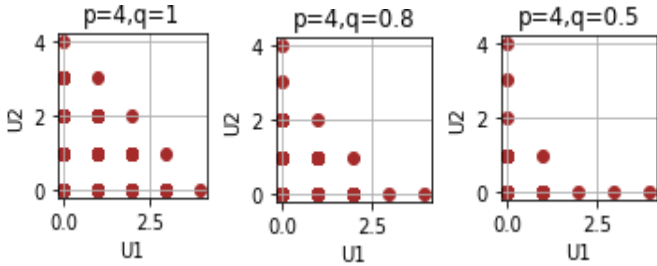
Figure 2 The retained basis terms with full expansion (q=1) and after truncation (q=0.8, q=0.5) are shown pictorially for polynomial expansion of order 4. First two dimensions are considered in X & Y axis respectively. X & Y axes represent the degree of the polynomials in each dimension.

3. ANALYSIS SETUP

For the uncertainty study, an offshore vessel named Olympic Challenger is chosen. In this regard, a representative numerical model of the same which is compatible with Wamit based hydrodynamic analysis has been utilized. The details of the model are summarized in the Table 1 [19].

The real vessel data, latitude & longitude, time and heading of the Olympic Challenger are utilized for the present study. Metocean conditions for the corresponding vessel position and time are read from the C3S-CDS ERA 5 reanalysis dataset [12]. The given vessel's position and time did not exactly coincide with the ERA 5 grid, so linear interpolation is used to find the metocean parameters at the same location & time as of the real asset. ($Hs - 3.1m, Tp - 10.35\ s, \theta_M - 226\ deg$). Panel model of the vessel is displayed in Figure 3. Positive X-axis points forward (x=0 at Lpp/2), positive Y-axis is pointing towards port side and positive Z-axis points upwards with z = 0 in the still water plane.
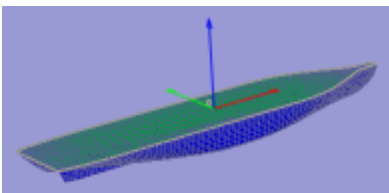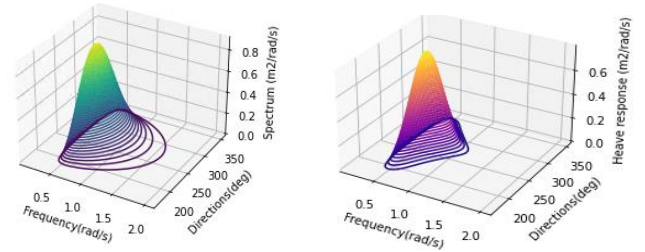

Figure 3 Panel model of the vessel

Table 1 Details of the numerical vessel model

Length, LOA	105.9 m
Length, Lpp	94.7 m
Breadth,B	21 m
Draught, T	6.28 m
Volume	8999 m^3
Waterplane Area	1842 m^2
Total no.of panels	3232
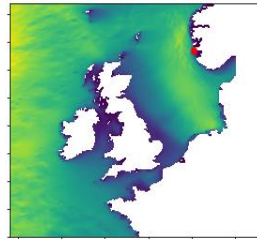
Figure 4 Location of the vessel is highlighted using red pointer. The vessel is positioned at lat-59.41°, lon – 5.26°and time – 08-01-2020T00:35:00. Vessel heading – 305.95 deg

Figure 5 Wave spectrum with $\gamma = 1$ and the resulting response spectrum for heave using the given sea state values, vessel heading and mean value of system parameters. 126 wave frequencies and 37 wave directions are used in the spectra.

The frequency domain analysis accounting for short crested seas represents the primary high-fidelity analysis. For conducting simulations, the numerical setup has to be fed with metocean, vessel heading and system parameters as input. The 2D wave spectrum and the resulting 2D heave response spectrum, simulated based on the high-fidelity analysis using the given sea states, vessel heading and mean value of system parameters are shown in Figure 5. 2D spectra are built using 126 wave frequencies and 37 wave directions. By using trapezoidal integrations, the response RMS is obtained as per the procedure stated in Section 2.1. Same steps are followed to estimate the response RMS, the quantities of interest, for all rigid body modes.

The method for assessing the sensitivity of the vessel QoIs by a surrogate follows a two-step process. Firstly, the stochastic output resulting from uncertain inputs has to be propagated into the surrogate model. This entails assigning random distributions to the uncertain inputs. The distributions for each input quantities are listed in Table 2. The mean and standard deviation ranges are approximately adapted from Han et al. (2020), where these ranges are proposed for a similar offshore vessel [20].

Table 2 Summary of uncertain system parameters together with their respective distributions. The explanation of the terminologies used are given below the table.

$XCG(m)$	Normal($\mu = -1.38$, $\sigma = 0.71\%$ of Lpp)
$YCG(m)$	Normal($\mu = 0, \sigma = 0.8\%$ of B)
$ZCG(m)$	Normal($\mu = 1.7, \sigma = 2.66\%$ of T)
$M(kg)$	Normal($\mu = 9223770, \sigma = 1.67\%$ of μ)
$I_{44}(kgm^2)$	Normal($\mu = 6.14x10^8, \sigma = 1.67\%$ of μ)
$I_{55}(kgm^2)$	Normal($\mu = 6.28x10^9, \sigma = 1.67\%$ of μ)
$I_{66}(kgm^2)$	Normal($\mu = 6.25x10^9, \sigma = 1.67\%$ of μ)
$\beta_{33}(\frac{kg}{s})$	Normal($\mu = 8\%\ \beta_{33,cr}, \sigma = 1.33\%\ \beta_{33,cr}$)
$\beta_{44}(kg\frac{m^2}{s})$	Normal($\mu = 9\%\ \beta_{44,cr}, \sigma = 1.17\%\ \beta_{44,cr}$)
$\beta_{55}(kg\frac{m^2}{s})$	Normal($\mu = 8\%\ \beta_{55,cr}, \sigma = 1.33\%\ \beta_{55,cr}$)

$\beta_{yy,cr} = 2\sqrt{(\overline{\overline{M}} + \overline{\overline{A}}_{yy})\overline{\overline{C}}_{yy}}$, yy = 3,4,5

CoG Center of Gravity
XCG Longitudinal coordinate of CoG
YCG Transverse coordinate of CoG

ZCG Vertical coordinate of ZCG
M Vessel mass
I_{44} Roll moment of inertia
I_{55} Pitch moment of inertia
I_{66} Yaw moment of inertia
β_{33} Additional linearized heave damping coefficient
β_{44} Additional linearized roll damping coefficient
β_{55} Additional linearized pitch damping coefficient
$\beta_{33,cr}$ Critical heave damping coefficient
$\beta_{44,cr}$ Critical roll damping coefficient
$\beta_{55,cr}$ Critical pitch damping coefficient

Estimation of the joint distribution is carried out using N marginals listed in Table 2, with the assumption that the variables are independent. This signifies the physical space of input variables. Here, only the system parameters are modelled as random variables, whereas the sea state parameters are kept deterministic. Parallelly, a joint distribution, consisting of N standard independent normal marginals, is formed and herein referred to as the standard normal space. In succession, orthogonal polynomials belonging to the Hermite family are generated with respect to the standard normal space using a three terms recursion scheme. By deploying Sobol' sampling, a low discrepancy/quasi-random scheme, samples are drawn from the normal space. Now, the normal samples are transformed to produce physical space samples based on the formulation $x = F_X^{-1}(F_U(u))$ [1]. In one case study, correlation between the variables in the physical space is also considered. For that analysis, the samples are generated from physical space and transformed to normal space by the formulation $u = F_U^{-1}(F_X(x))$ [21]. Usage of Rosenblatt transformation is considered. The high-fidelity model is run using the physical samples.
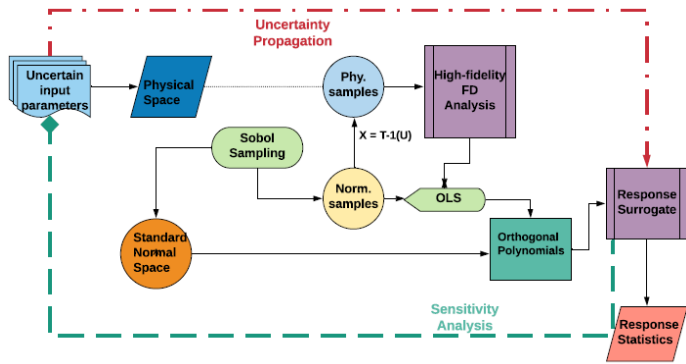
Figure 6 Illustrative flowchart showing the sequential procedure followed for performing polynomial surrogate based sensitivity analysis

Afterwards, using the random response output from the high-fidelity model and the standard normal samples, the coefficients of the orthogonal polynomial sequence are estimated by employing a least squares minimization strategy. This first-step, consequently, results in engendering of a response surrogate that can mimic the behaviour of the high-fidelity model. In this manner, the PC surrogate is built for all response QoIs. The

second-step, performing sensitivity analysis, can be initiated by decomposing the coefficients of the polynomial surrogate. A graphical illustration of the work sequence is shown by a flowchart in Figure 6. The whole analysis has been carried out with the help of Python based packages [22] [23] [24].

4. RESULTS AND DISCUSSION

4.1 Convergence Study

With the aim of attaining reliable sensitivity results, a full-fledged convergence study is performed to ensure the usage of the optimal number of high-fidelity runs and polynomial order for performing sensitivity analysis. In total, there are 10 random variables used for the sensitivity study. The number of generated terms, therefore, in respect of each polynomial order along with their truncated versions are presented in Table 3.

Table 3 Number of generated terms with respect to different polynomial versions

Pol	P2	P3	P3 q-0.8	P4	P4 q-0.8	P4 q-0.5
Terms	66	286	76	1001	296	86

By using the mean and standard deviation obtained from the polynomial coefficients associated with the surrogate built for roll RMS, the confidence interval$(\mu \pm \sigma)$ is constructed for various ranges of high-fidelity runs starting from 50 to 1000. Though for OLS, the minimum number of simulation samples required should be higher than the number of polynomial terms, the mean and standard deviation for all the polynomial surrogates, irrespective of the number of terms they posses,are presented for all sample numbers inorder to justify the convergence study. From the plots, the full 2nd order polynomial with 66 terms has reached convergence from 100 runs onwards and remained stable throughout. Inaddition, Monte Carlo runs on the high-fidelity model are also conducted and the confidence intervals are presented until 10000 runs. The mean and standard deviation of full 2nd order polynomial surrogate with 100 runs are 2.077 & 0.282 deg respectively, and the Monte Carlo results for 10000 runs show values of 2.081 & 0.287 deg respectively for mean and standard deviation. Thereby, the full PC model of order 2 has been chosen for further studies. Concerning the number of high-fidelity runs required to train the surrogate model, 200 runs is selected for constructing surrogates for all rigid body modes. Even though the convergence has been achieved earlier for roll in Figure 7, the selection is based on a conservative assumption. Moreover, the choice of 2nd order polynomial with 66 terms and 200 simulation runs also satisfies the qualitative thumb rule condition.

The truncated polynomial candidates (q=0.5) corresponding to PC model of order 2 and 3 achieved convergence before the full PC 2nd order model. However, they produced identical values for the first order and total sensitivity indices for all the modes. In other words, they did not capture the small interaction effects

existing between the variables for certain modes. The related results are presented in the Appendix section.
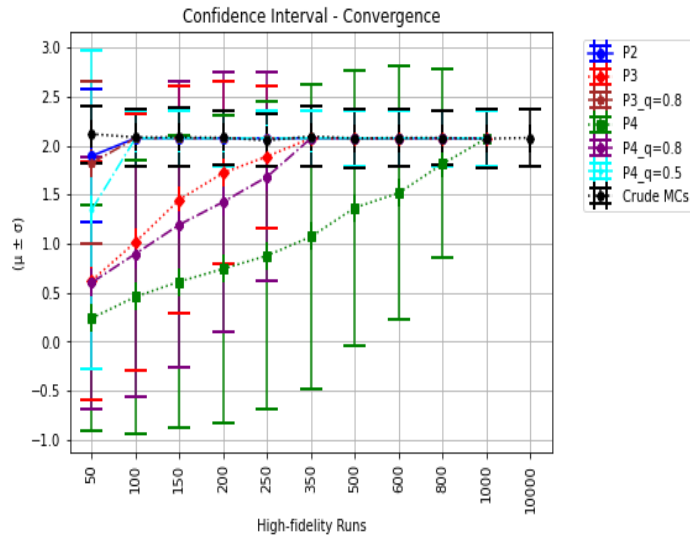
Figure 7 Convergence rate of different polynomial versions with respect to different number of high-fidelity simulation runs(50-1000). In addition, crude MonteCarlo runs are conducted on the high-fidelity model and results are presented for samples ranging from 50-10000.

With the main intention to present the interactions between the variables using a PC model that requires least number of runs, full PC expansion of order 2 that reached convergence sooner is chosen. Notwithstanding, if only the prediction of main effects (first order indices) is important in a study, truncated PC expansions can be efficiently used.

### 4.2 Sensitivity of rigid body motions due to system uncertainty.

The first order and total order indices are presented for all rigid body modes in Figure 8. 2% value of the respective index is added on top of each index as confidence interval inorder to mark the uncertainty associated with the choice of distributions considered for the input parameters. The analysis takes into account the relative wave heading at 259.96°, which could be regarded as a beam sea. Therefore, many system parameters seem to contribute to the response variation in sway, roll and yaw motions, as these are the responsive modes in a beam sea. The CoG parameters, most importantly, are significantly contributing to the response variation in 2,4,6 modes, as these parameters are present in the mass and stiffness matrices and are responsible for the changes in mean wetted surface.

With regards to the heave and pitch motion, almost 97.2% and 96.5% of the response variations are driven by their respective damping coefficients alone, with trivial contributions from other parameters. The vessel mass imparts substantial variation in translational modes. This applies, especially in surge and sway, where it bestows around 52.7% and 48.3% variations respectively. Likewise, the yaw moment of inertia drives 47.7%

of the yaw variation. However, relevant moments of inertia in roll and pitch motion fail to impart considerable effect. In physical conditions, the motion modes 1,3,5 and 2,4,6 are integrated. The sensitivity indices clearly depict the interrelations, for instance, β_{55} appears to influence almost 34.2% variation in surge response, roll moment of inertia exercises little effect (1.64%) on sway motion and β_{33} offers slight variations to pitch response.
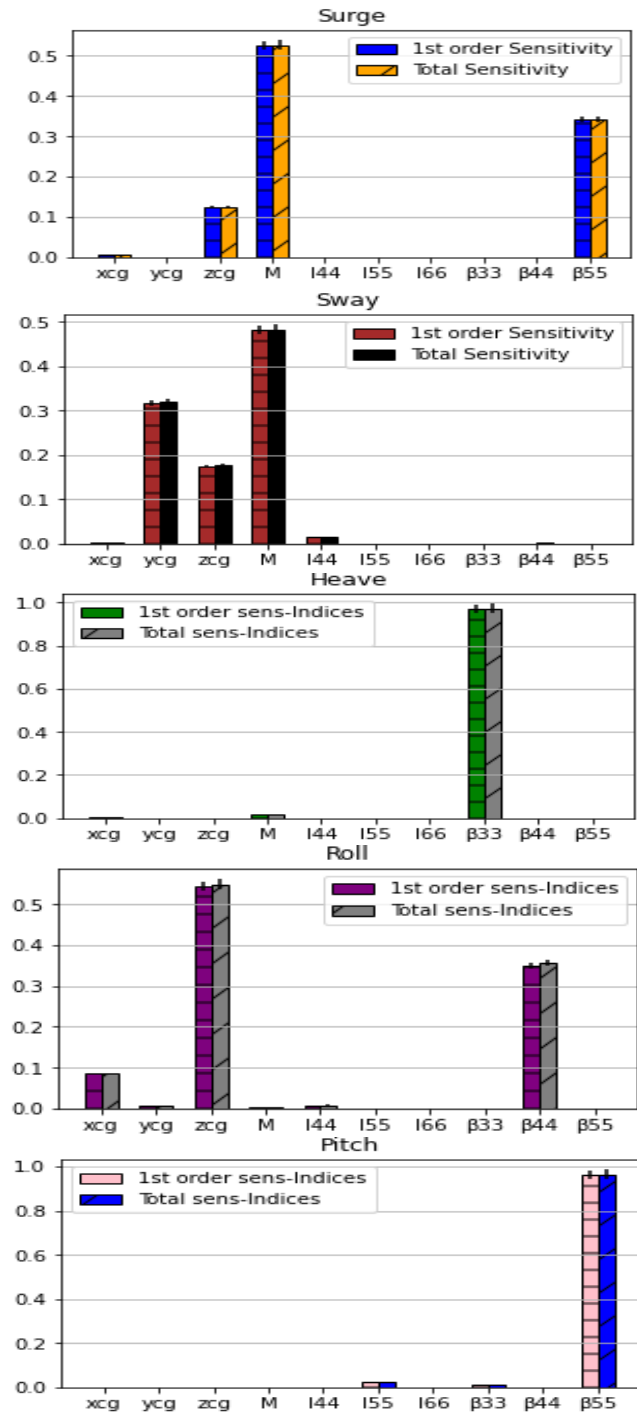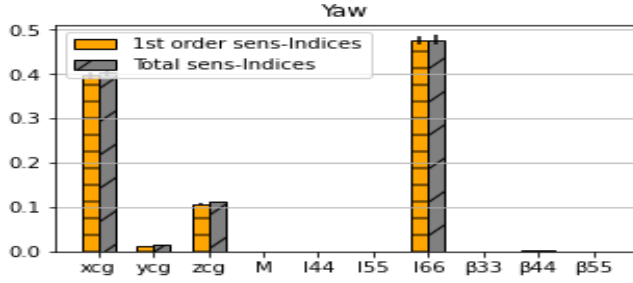
Figure 8 First order and total order sensitivity indices are presented consecutively for each rigid body motion – 1. Surge, 2. Sway, 3. Heave, 4. Roll, 5. Pitch, 6. Yaw. 200 High fidelity runs are made to construct the surrogate

Interactions, however negligible, are also present between the parameters for 2,4,6 motion modes, which is evident from the slightly higher total indices than the corresponding first order indices. For illustration, the roll damping and ZCG in roll mode are faintly interacting with each other, as second order index with 0.6% is present for these parameters. Nevertheless, for all modes, contributions from the first order indices are mostly dominating, signifying that the coefficients related to the interaction terms are inconsequential compared to the main terms. Figure 9 showing the polynomial coefficients for all the modes explain the trifling higher order terms with little/nil fluctuations.
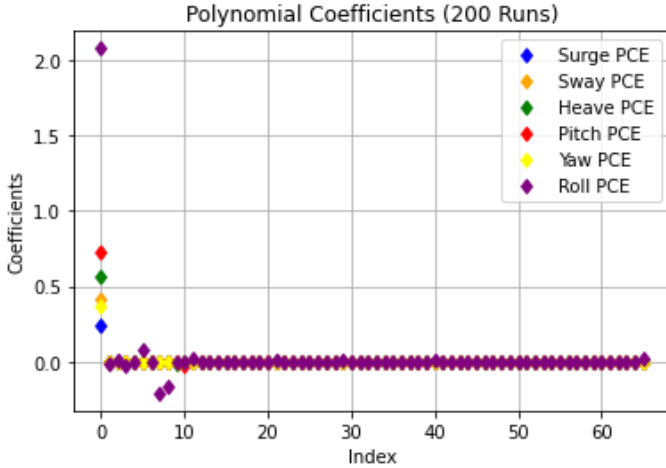
Figure 9 Polynomial coefficient values from the surrogates of 6 rigid body modes. Surrogate built from the full polynomial expansion of order 2 trained with 200 samples.

The sensitivity indices appear to be highly dependent upon the chosen uncertainty ranges of the system parameters and their values may vary with the increase in the uncertainty range.

Besides the sensitivity indices, the statistical moments and the 95% value are evaluated from the polynomial coefficients and presented in Table 4. For the considered sea state values, all other rigid body modes, except roll, exhibit insignificant scattering from the mean value. Especially sway mode, which shows very low level of scatter, despite receiving contributions from many system parameters. Roll motion shows 13.6% deviation from the

mean value, which is quite considerable. The numeric figures related to higher order moments indicate that all the response modes tend to reflect the Gaussian nature, however, the roll response is slightly deviating from the Gaussian behaviour.

Table 4 Statistical moments and 95% RMS value from the polynomial surrogates corresponding to each rigid body motion. Units of surge, sway and heave are in 'm', and of roll, pitch and yaw are in 'deg'. Skewness and kurtosis are dimensionless quantities.

	Surge	Sway	Heave	Roll	Pitch	Yaw
Mean	0.242	0.415	0.56	2.077	0.722	0.372
STD	0.005	0.006	0.014	0.283	0.022	0.006
Skewness	0.095	0.079	0.162	0.278	0.193	0.102
Kurtosis	3.013	3.037	3.035	3.210	3.050	3.060
95 % val.	0.254	0.435	0.603	3.432	0.784	0.401

4.3 Roll RMS variation to β_{44} increments

Using three different cases, the response sensitivity to β_{44} increments is studied using statistical measures in this section. The first case is run using the same random parameters as listed in Table 2. In the next two cases, the mean value of β_{44} is supplemented with additional 5% sequentially, while the standard deviation is kept the same. 95% roll RMS value read from the polynomial coefficients, evidently, indicates that the increase of β_{44} to 5% suppresses the roll exterme RMS by around 15-20%. It can seen in Table 5.

Table 5 Statistical moments & 95% RMS value obtained from polynomial coefficients corresponding to roll surrogate

|	$\mu = 9\% \beta_{44,cr}$	$\mu = 14\% \beta_{44,cr}$	$\mu = 19\% \beta_{44,cr}$
Mean	2.077 deg	1.563 deg	1.269 deg
STD	0.283 deg	0.185 deg	0.139 deg
Skewness	0.278	0.171	0.147
Kurtosis	3.210	3.109	3.086
95% value	3.43 deg	2.68 deg	2.27 deg

.
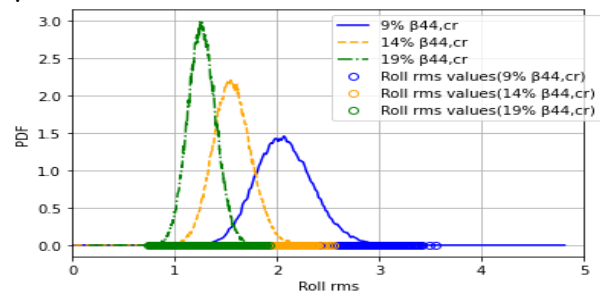
Figure 8 Response PDF constructed for the considered three cases using the Gaussian kernel associated with the kernel density estimation. 100,000 RMS values simulated from the respective surrogates are displayed in the X-axis

Additionally, the response PDF is constructed for each case by performing 100,000 runs on the respective PC model and enveloping the obtained results with a Gaussian kernel. The curves are displayed in Figure 10. PDF curves attained from the

kernel density estimation clearly portray 18-25% reduction in the mean value of roll response together with higher concentration of responses adjacent to the mean for increasing β_{44} values. In like manner, the higher order moments given in Table 5, suggest that the roll behaves more Gaussian with β_{44} increments

4.4 Effect on sensitive indices on introduction of artificial correlation

In the previous cases, assumption of independence between the variables is considered on account of the fact that the actual correlation between system variables is not known. From a physical perspective, some of the variables are correlated to each other, and consequently the correlation might influence the resulting response. In the current section, thereby, the model response sensitivity is assessed by introducing artificial correlation. For sway motion, three different cases are studied. One with the assumption of independence between the variables as before, whereas the other two cases have been assigned with 15% and 30% correlations respectively. A multivariate normal distribution, assigned with the prescribed correlations between the paramters XCG,YCG,ZCG,M, I_{44} , β_{44} and zero correlation for rest of the variables, is utilized. Only the parameters that may induce changes to the sway response are selected for prescribing correlation, whereas the parameters having nil/negligible effects are given zero correlation. This selection is duly based on the results presented in Section 4.2.
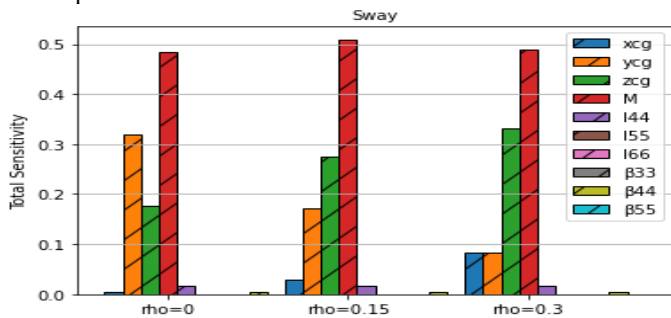
Figure 9 For three different correlation cases, total sensitivity indices for all input paramters are given for sway RMS.

Table 6 Statistical moments obtained from the polynomial coefficients corresponding to the sway surrogate

|	$\rho = 0$	$\rho = 0.15$	$\rho = 0.3$
Mean	0.4146 m	0.4146 m	0.4147 m
Std	0.006 m	0.006 m	0.006 m
Skewness	0.079	0.125	0.198
Kurtosis	3.037	3.065	3.121

A representation of the total sensitivity indices for the three cases is given in Figure 11. The gradual enhancement of 15% correlation results in a 11-14% corresponding decline in the total effect of YCG on sway response. In contrast, the sheer contribution of XCG and ZCG to system response variation escalates with the stepwise accumulation of correlation. The total index corresponding to other parameters did not display any

substantial changes. Thus, it leads to the conclusion that correlation directly influences only the importance of the CoG parameters on the system response.

Table 6 containing higher order moments suggests a faint deviation of the sway response from the Gaussian behaviour with respect to increased correlation. Numerical figures on mean and standard deviation imply that they are not reactive to the increase in correlation, which is indicative of the fact that the overall sway RMS is not affected much by the presence of correlation.

4.5 Response sensitivity to variations in incoming wave directions

All the previous analyses exclusively take into account a relative wave direction of 259.96° . In continuation, the parametric effect on system response in relation to various relative directions have been studied in detail. 7 different cases are studied keeping Hs and Tp the same as before, but relative directions(θ_R) are changed from 0 to 180° in intervals of 30°. In Figure 12, for each rigid body motion, the total sensitivity indices corresponding to each incoming wave direction are presented. As can be seen, sway, roll and yaw modes are highly responsive to the changes in the wave directions.
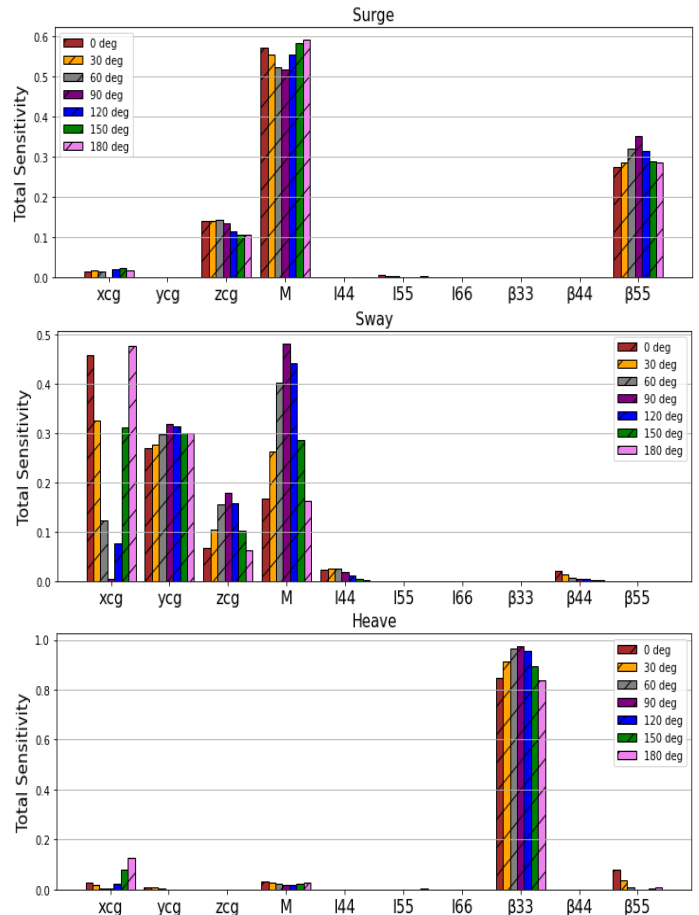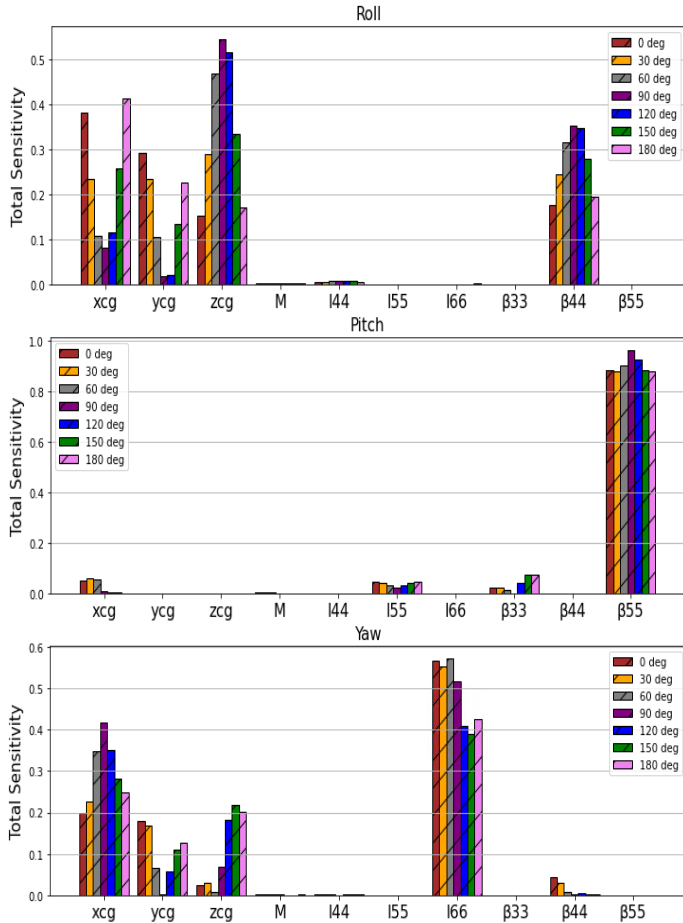
Figure 10 Total sensitivity indices corresponding to different relative directions are presented for all rigid body motions. 1. Surge, 2. Sway, 3. Heave, 4. Roll, 5. Pitch, 6. Yaw.

Massive changes in the importance of parameters can evidently be witnessed for these modes. Take for instance, in quantative terms, for sway mode, the Xcg parameter contributes to just 0.4% of response variation in beam seas. In sharp contrast, the same parameter is responsible for causing around 47.6% and 45.8% variations in head and following seas respectively. In addition, ZCG and vessel mass also exhibit directional dependency, presenting substantial effects on sway response in beam seas, but, showing a decreasing trend for other directions. In a similar fashion, abrupt changes in the CoG parameters and damping coefficient are clearly visible for the roll mode. The ZCG bestows more than 54 % response variation for waves approaching at 90°, while it contributes only around 15 % and 17% response variation for waves arriving at 0° and 180° respectively. XCG shows kindred effects for sway and roll, (i.e), displaying symmetrically increasing behaviour with minimum at 90°, while, a symmetrically decreasing trend with a maximum at 90° can be witnessed for the yaw mode. 2,4,6 are the most reactive modes in beam seas, thus, most of the parameters have, either a maximum or minimum at 90°. Apart from these, parameters corresponding to modes like surge, heave and pitch do not demonstrate appreciable modifications and remain less reactive to directional changes. Only some CoG and damping coefficient parameters exhibit slight variations. Thus, it leads to the conclusion, that the parameters associated with the response variations in modes 1,3,5 have little sensitivity to the wave directions.

5. CONCLUSION

In this study, the Sobol' indices generated from polynomial coefficients were efficiently applied for measuring the contribution of each uncertain parameter on the response QoIs. Based on the convergence studies and also with the intent to capture interaction effects between the variables, full polynomial expansion of order 2 was selected. For the chosen sea state, the sway, roll and yaw modes, were most sensitive to the parametric uncertainty. Specifically, significant level of scatter was observed for roll motion, thereby, deeming it the most critical parameter affected by the system uncertainties. Furthermore, the variations of the roll response on exposure to different mean value ranges of β_{44} were considerable, and as a consequence, the calibration of β_{44} is considered extremely vital for reliable roll response prediction. CoG parameters and roll damping coefficient appeared to be heavily dependent on wave directions. Specifically, extreme changes in the contributions of CoG parameters to response variation were observed for different directions. The results, therefore, stress the need to switch the parameters while performing surrogate assisted model calibration with respect to different incoming wave directions. All the analyses, in this study, have been conducted using a deterministic value for Hs & Tp. A further extension would be to model all the metocean parameters as random variables and quantitatively measure the resulting interactions between system and metocean parameters. This would pave the way for identification of the sea state dependent system parameters, and consequently, would facilitate reliable model calibration.

REFERENCES

[1]   B. Sudret, "Global sensitivity analysis using polynomial chaos expansions," *Reliability Engineering & System Safety,* pp. 964-979, 2007.

[2]   G. Blatman, "Adaptive sparse polynomial chaos expansions for uncertainty propagation and sensitivity

analysis," Institut Francais de Mecanique Avancee et Universite Blaise Pascal, 2009.

[3] G. Deman, K. Konakli, B. Sudret, J. Kerrou, P. Perrochet and H. Benabderrahmane, "Using sparse polynomial chaos expansions for the global sensitivity analysis of groundwater lifetime expectancy in a multi-layered hydrogeological model," *Reliability Engineering and System Safety,* no. 147, pp. 156-169, 2016.

[4] C. V. Mai, "Polynomial chaos expansions for uncertain dynamical systems - Application in earthquake engineering," ETHZ, Zurich, 2016.

[5] T. Sauder, "Fidelity of cyber-physical empirical methods - Application to the active truncation of slender marine structures," Norwegian University of Science and Technology, Trondheim, 2018.

[6] P. Ni, J. Li, H. Hao and Y. Xia, "Stochastic dynamic analysis of marine risers considering Gaussian system uncertainties," *Journal of Sound and Vibration,* no. 416, pp. 224-243, 2017.

[7] G. M. Paredes, C. Eskilsson and A. P.Engsig-Karup, "Uncertainty quantification in mooring cable dynamics using polynomial chaos expansion," *Journal of Marine Science and Engineering,* vol. 8, no. 162, pp. 1-23, 2020.

[8] X. Wei, H. Chang, B. Feng and Z. Liu, "Sensitivity analysis based on Polynomial Chaos Expansions and its application in ship uncertainty based design optimization," *Mathematical Problems in Engineering,* pp. 1-19, 2019.

[9] DNV-GL, "Recommended practice DNV-RP-C205 Environmental Conditions and Environmental Loads," DNV, 2010.

[10] Coastal Engineering Research Center , "Coastan Engineering Technical Note - Directional wave spectra using cosine-squared and cosine 2S spreading functions," U.S Army Engineer Waterways Experiment Station, Mississippi, 1985.

[11] D. Skandali, "Identification of response amplitude operators for ships based on full scale measurements," TU Delft, Delft, 2015.

[12] H. Hersbach, B. Bell, P. Berrisford, G. Biavati, A. Horányi, J. Muñoz Sabater, J. Nicolas, C. Peubey, R. Radu, I. Rozum, D. Schepers, A. Simmons, C. Soci, D. Dee and J.-N. Thépaut, "ERA5 hourly data on single levels from 1979 to present.," Copernicus Climate Change Service (C3S) Climate Data Store (CDS), 2018. [Online]. Available: https://cds.climate.copernicus.eu/cdsapp#!/dataset/rean alysis-era5-single-levels?tab=form. [Accessed 15 December 2020].

[13] Z. Gao, "Lecture notes - Frequency and time domain stochastic analysis of wave induced dynamic responses," Norwegian University of Science and Technology, Trondheim, 2020.

[14] J. Journee and WW.Massie, Offshore Hydromechanics, Delft: Delft University of Technology, 2001.

[15] WAMIT, Inc, "WAMIT User Manual," Massachusetts Institute of Technology, Chestnut Hill, MA, 2013.

[16] A. Saltelli, M. Ratto, T. Andres, F. Campolongo, J. Cariboni, D. Gatelli and S. T. M. Saisana, Global Sensitivity Analysis. The Primer, Chichester; West Sussex: John Wiley & Sons, Ltd, 2008.

[17] T. Homma and A. Saltelli, "Importance measures in global sensitivity analysis of nonlinear models," *Reliability Engineering and System Safety,* no. 52, pp. 1-17, 1996.

[18] B. Sudret, "Uncertainty propagation using polynomial chaos expansions," Chair of Risk, Safety and Uncertainty Quantification, ETH Zurich, Weimar, 2016.

[19] F. Solaas, "SIMA model of Olympic Challenger," SINTEF Ocean AS, Trondheim, 2019.

[20] X. Han, S. Sævik and B. J. Leira, "A sensitivity study of vessel hydrodynamic model parameters," in *Proceedings of ASME 2020 39th International Conference on Ocean, Offshore and Arctic Engineering*, Virtual, 2020.

[21] E. Torre, S. Marelli, P. Embrechts and B. Sudret, "Data-driven polynomial chaos expanison for machine learning regression," *Journal of Computational Physics,* vol. 388, pp. 601-623, 2019.

[22] H. P. L. Jonathan Feinberg, "Chaospy: An open source tool for designing methods of uncertainty quantification," *Journal of Computational Science,* vol. 11, pp. 46-57, 2015.

[23] J. Feinberg, "Chaospy documentation," Chaospy, 2020. [Online]. Available: https://chaospy.readthedocs.io/en/master/. [Accessed 15 December 2020].

[24] SciPy community, "SciPy Reference Guide Release 1.6.0," 31 December 2020. [Online]. Available: https://docs.scipy.org/doc/scipy-1.6.0/scipy-ref-1.6.0.pdf. [Accessed 5 January 2021].
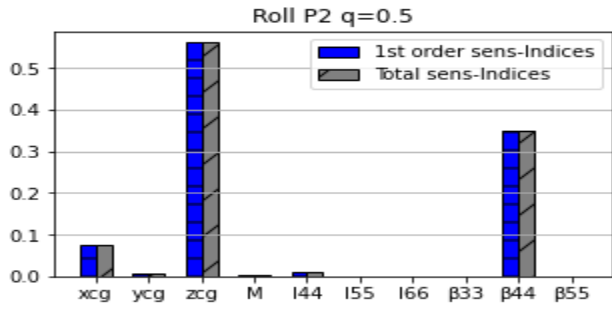
APPENDIX

Figure 11 First order and total sensitivity indices for Roll RMS. Truncated version of 2nd order PC model with 21 terms is used. 50 simulation samples are utilized to train the surrogate. As can be seen, the truncated version fails to capture the interaction between the variables.
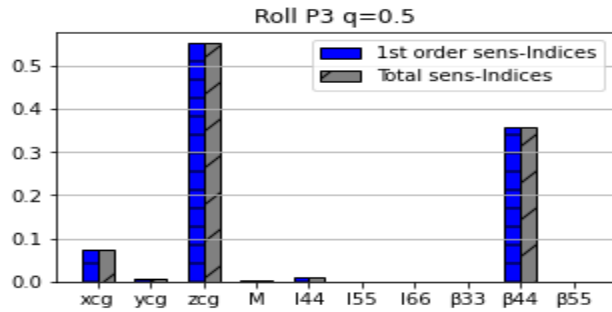

Figure 12 First order and total sensitivity indices for Roll RMS. Truncated version of 3nd order PC model with 31 terms is used. 100 simulation samples are utilized to train the surrogate. The total indices are identical to the first order indices indicating that the interactions are absent.